Title

^{18}F-FAC PET Selectively Images Liver-Infiltrating CD4 and CD8 T Cells in a Mouse Model of Autoimmune Hepatitis.

Journal

Journal of nuclear medicine : official publication, Society of Nuclear Medicine, 59(10)

ISSN

0161-5505

Authors

Salas, Jessica R
Chen, Bao Ying
Wong, Alicia
et al.

Publication Date

2018-10-01

DOI

10.2967/jnumed.118.210328

Peer reviewed

Journal of Nuclear Medicine, published on April 26, 2018 as doi:10.2967/jnumed.118.210328

^{18}F-FAC PET selectively images hepatic infiltrating CD4 and CD8 T cells in a mouse model of autoimmune hepatitis

Jessica R. Salas[1,2], Bao Ying Chen[1,2], Alicia Wong[1,2], Donghui Cheng[3], John S. Van Arnam[5], Owen N. Witte[1,3,4], Peter M. Clark[1,2,3,‡]

[1] Department of Molecular and Medical Pharmacology, [2] Crump Institute for Molecular Imaging, [3] Eli and Edythe Broad Center of Regenerative Medicine and Stem Cell Research, [4] Department of Microbiology, Immunology, and Molecular Genetics, University of California, Los Angeles, CA 90095. [5] Department of Pathology and Laboratory Medicine, University of Pennsylvania, Philadelphia, CA 19104

‡ Correspondence should be addressed to Peter M. Clark, Crump Institute, Box 951770, 4333 CNSI, Los Angeles, CA 90095-1770; 310-267-4755; pclark@mednet.ucla.edu

First author: Jessica R. Salas, Crump Institute, Box 951770, 4333 CNSI, Los Angeles, CA 90095-1770; 310-267-4755; cunninj20@k-state.edu (Researcher)

Word count: 5,000

Financial support: Support for this study was provided by the NIH, the Parker Institute for Cancer Immunotherapy, and the Broad Stem Cell Research Center at UCLA. PMC and ONW are inventors on a patent, held by the Regents of the University of California, that describes the ^{18}F-DFA radiotracer. ONW is an inventor on a patent, held by the Regents of the University of California, that describes the ^{18}F-FAC radiotracer.

Running title: Imaging liver lymphocytes with ^{18}F-FAC

Abstract

Immune cell-mediated attack on the liver is a defining feature of autoimmune hepatitis and hepatic allograft rejection. Despite an assortment of diagnostic tools, invasive biopsies remain the only method for identifying immune cells in the liver. We evaluated whether PET imaging with radiotracers that quantify immune activation (^{18}F-FDG and ^{18}F-FAC) and hepatocyte biology (^{18}F-DFA) can visualize and quantify hepatic infiltrating immune cells and hepatocyte inflammation, respectively, in a preclinical model of autoimmune hepatitis. **Methods.** Mice treated with Concanavalin A (ConA) to induce a model of autoimmune hepatitis or vehicle were imaged with ^{18}F-FDG, ^{18}F-FAC, and ^{18}F-DFA PET. Immunohistochemistry, digital autoradiography, and *ex vivo* accumulation assays were used to localize areas of altered radiotracer accumulation in the liver. For comparison, mice treated with an adenovirus to induce a viral hepatitis or vehicle were imaged with ^{18}F-FDG, ^{18}F-FAC, and ^{18}F-DFA PET. ^{18}F-FAC PET was performed on mice treated with ConA, and vehicle or dexamethasone. Biopsy samples of patients suffering from autoimmune hepatitis were immunostained for deoxycytidine kinase (dCK). **Results.** Hepatic accumulation of ^{18}F-FDG and ^{18}F-FAC was 173% and 61% higher, respectively, and hepatic accumulation of ^{18}F-DFA was 41% lower in a mouse model of autoimmune hepatitis compared to control mice. Increased hepatic ^{18}F-FDG accumulation was localized to infiltrating leukocytes and inflamed sinusoidal endothelial cells, increased hepatic ^{18}F-FAC accumulation was concentrated in infiltrating CD4 and CD8 cells, and decreased hepatic ^{18}F-DFA accumulation was apparent in hepatocytes throughout the liver. In contrast, viral hepatitis increased hepatic ^{18}F-FDG accumulation by 109% and decreased hepatic ^{18}F-DFA accumulation by 20% but had no effect on hepatic ^{18}F-FAC accumulation (non-significant 2% decrease). ^{18}F-FAC PET provided a non-invasive biomarker of the efficacy of dexamethasone for treating the autoimmune hepatitis model.

Infiltrating leukocytes in liver biopsy samples from patients suffering from autoimmune hepatitis express high levels of dCK, a rate-limiting enzyme in the accumulation of ^{18}F-FAC. **Conclusions.** Our data suggests that PET can be used to non-invasively visualize activated leukocytes and inflamed hepatocytes in a mouse model of autoimmune hepatitis.

Key words: PET imaging, autoimmune disease, hepatitis, hepatocytes

Introduction

Immune cell infiltration into the liver and attack on liver cells is characteristic of various pathologies, including autoimmune hepatitis and hepatic allograft rejection (*1*,*2*). Immune-mediated attack on the liver can lead to significant cellular damage, and hepatic allograft rejection is a leading cause of liver re-transplantation (*1–4*). T lymphocytes make up a sizable fraction of the hepatic infiltrating leukocytes in autoimmune hepatitis and hepatic allograft rejection, and various animal models suggest a critical role for T lymphocytes in these diseases (*5–9*).

Current clinical methods for evaluating hepatocyte inflammation and hepatic-infiltrating T lymphocytes *in vivo* are valuable but provide an incomplete picture of disease (*10–17*). Hepatocellular damage can be inferred from blood levels of enzymes and metabolites enriched in or processed by the liver, including alanine transaminase (ALT), aspartate transaminase (AST), and bilirubin. However these measures do not always accurately reflect the degree of hepatic-infiltrating T lymphocytes and are not predictive of disease reversibility (*10*,*11*). The liver can also be imaged by computed tomography (CT), magnetic resonance imaging (MRI), and ultrasound but these imaging modalities provide limited functional information (*12*). Blood CD4 T cell intracellular ATP levels, measured *ex vivo* after stimulation, may provide information on immune activation in the setting of a liver transplant, but the sensitivity and specificity of this approach remains controversial, and this approach provides no direct information on lymphocyte activity specifically in the liver (*13*). Liver biopsies remain the gold standard for assessing hepatic infiltrating lymphocytes but suffer significant sampling error, carry a risk of complications, and are often challenging to interpret in diseases with heterogeneous manifestations such as hepatic allograft rejection (*14–17*). A method to selectively quantify and visualize CD4 and CD8 T lymphocytes and inflamed hepatocytes in the liver within the context of

autoimmune hepatitis and hepatic allograft rejection could improve our understanding of these diseases and function as a potential biomarker of therapy.

We recently developed a family of PET imaging radiotracers – ^{18}F-2-deoxy-2-fluoroarabinose (^{18}F-DFA) and ^{18}F-2-deoxy-2-fluororibose (^{18}F-2-DFR) – that measure ribose salvage activity, a pathway highly upregulated in liver hepatocytes (*18*,*19*). We showed that ^{18}F-DFA PET quantifies functional hepatocyte density in a mouse model of drug-induced acute liver failure and that hepatic ^{18}F-DFA accumulation is decreased in mouse models of fatty liver disease (*18–20*). Alternatively, the PET radiotracers ^{18}F-FDG and ^{18}F-1-(2'-deoxy-2'-fluoro-arabinofuranosyl)cytosine (^{18}F-FAC) measure glucose consumption and deoxynucleoside salvage, respectively, two processes upregulated during immune cell activation (*21–23*). ^{18}F-FDG and ^{18}F-FAC PET can monitor immune activation in mouse models of systemic autoimmune disease, colitis, and immune-mediated tumor rejection (*22–26*). Consistent with studies indicating that PET can be used to image autoimmune disease in other organ systems (*27–29*), previous studies suggest that hepatic ^{18}F-FDG accumulation is increased in a mouse model of autoimmune hepatitis and a rat model of hepatic allograft rejection (*30*,*31*), although the precise cellular source of this increased accumulation remains unclear.

Here, we study ^{18}F-FDG, ^{18}F-FAC, and ^{18}F-DFA in mouse models of autoimmune and viral hepatitis. ^{18}F-DFA instead of ^{18}F-2-DFR was chosen here because ^{18}F-DFA can be synthesized on an automated radiosynthesizer and its radiochemical precursor is commercially available (*32*). Our results suggest that PET imaging with radiotracers that measure ribose and deoxynucleoside salvage could be used to image and quantify hepatocyte inflammation and hepatic infiltrating T lymphocytes during autoimmune hepatitis.

Materials and Methods

Mice: Male Balb/c (8 – 10 weeks old) and NSG (8 – 10 weeks old) mice were used for the ConA experiments. Male FVB (8 – 10 weeks old) and NSG (8 – 10 weeks old) mice were used for the adenovirus experiments. Balb/c and NSG mice were from an internal UCLA mouse breeding colony. FVB mice were from the Jackson Laboratory. All animal experiments were approved in advance by the UCLA Animal Research Committee.

Treatments: ConA: Mice were injected intravenous with saline vehicle or ConA (Type IV; 10 mg/kg; Sigma-Aldrich). Adenovirus: Mice were injected intravenous and intraperitoneal with a GFP-expressing adenovirus (100 microL each; titer: 5 x 10^8 PFU/mL; Cyagen). Dexamethasone: Mice were injected with 1X PBS vehicle or dexamethasone-21-phosphate (300 mg/kg) intraperitoneal 18 h and 1 h prior to the ConA injection.

Immunohistochemical analyses: Immunohistochemistry was performed as previously described (*20*) with the following exceptions: Antigen retrieval was performed in citrate antigen retrieval buffer (10 mM sodium citrate, pH 6.0) for dCK, GLUT1, CD4, CD8, CD11b, and Ki67 or a citrate-Tween 20 antigen retrieval buffer (10 mM sodium citrate, 0.05% Tween 20, pH 6.0) for B220. Slides were blocked in 2.5% horse serum (1 h, rt for GLUT1, CD8, B220, CD11b, and Ki67 or overnight, 4 °C for CD4) and incubated with primary antibody (overnight, 4 °C for GLUT1, CD8, B220, CD11b, and Ki67 or 1 h, rt for CD4; diluted in 2.5% horse serum). Antibodies and dilutions were as follows: dCK (developed by the Witte Lab, Clone 9D4; 1:1000), GLUT1 (Millipore, Clone 07-1401; 1:500), CD4 (Abcam, ab183685; 1:200), CD8 (eBiosciences, Clone 4SM15; 1:200), B220 (Biolegend, Clone RA3-6B2; 1:100), CD11b (Abcam, ab75476; 1:1000), Ki67 (Abcam, ab16667; 1:1000). Slides were wash in 1X PBS and incubated with horse anti-rabbit HRP (Vector Laboratories; 1 h, rt for GLUT1, CD4, CD11b, and Ki67) or treated with Elite ABC

complex following manufacturer's protocol (Vector Laboratories PK-6100; for B220 and CD8).

Liver sections from anonymized patients with autoimmune hepatitis were obtained from banked biopsy samples through the UCLA Translational Pathology Core Laboratory.

PET/CT imaging and quantification: PET imaging and quantification were performed as previously described (*20*). Briefly, anesthetized mice were injected with ~2.96 MBq (for the ConA experiments) or ~0.74 MBq (for the adenovirus experiments) and imaged 1 hr later by PET/CT for 10 minutes on a G8 PET/CT (Sofie Biosciences). ^{18}F-FDG was from the UCLA Translational Imaging Division. ^{18}F-FAC and ^{18}F-DFA were synthesized as previously described (*32*). Mice were injected with tracer approximately 30 hours after the ConA treatment. Mice were imaged 1 – 3 days prior to and then again 2, 4, 8, and 12 weeks after the adenovirus injections. Quantified PET images are reported as signal/background, where signal refers to radiotracer accumulation in the liver and background refers to radiotracer accumulation in a background organ (^{18}F-FDG: right forelimb triceps; ^{18}F-FAC and ^{18}F-DFA: brain).

Autoradiography: Autoradiography was performed as previously described (*20*). Frozen slides were fixed, stained for H&E, and digitally imaged.

Ex vivo accumulation assays: Mice were treated with ConA, as described above. Hepatic infiltrating leukocytes were isolated, sorted, and treated as previously described (*24*,*33*) except that the radiotracer ^{3}H-deoxycytidine (Moravek, Inc.) was used.

Statistical analyses: Data is plotted as mean with error bars representing standard error of the mean. Statistical analyses were performed using one-way and two-way ANOVA

with Tukey and Dunnett corrections, respectively, for multiple comparisons. Statistical analyses were performed by GraphPad Prism (Version 7.01).

Results

Hepatic ^{18}F-FDG, ^{18}F-FAC, and ^{18}F-DFA accumulation are affected in a mouse model of autoimmune hepatitis. The best-studied mouse model of autoimmune hepatitis is induced by treating mice with the plant lectin ConA (*9*). When injected into mice, ConA produces a CD4 T cell- and TNF-α-dependent but CD8 T cell-independent hepatitis (*9*,*34*). Mice injected with ConA exhibited a robust, periportal hepatitis, characterized by hepatic infiltrating leukocytes containing a high proportion of CD4 T cells (64 ± 2%) with additional contributions from CD11b-positive innate immune cells, B220-positive B cells, and CD8 T cells (9 ± 2%, 18 ± 2%, 13 ± 1%, respectively; **Fig. 1A**). A sizable fraction of the hepatic infiltrating leukocytes expressed Ki67 (67 ± 4%; **Fig. 1A**), a marker of cell proliferation. In agreement with literature (*30*), mice treated with ConA had significantly higher accumulation of hepatic ^{18}F-FDG compared to saline vehicle-treated mice (**Fig. 1B, C; Fig. S1**). Mice treated with ConA also exhibited higher levels of hepatic ^{18}F-FAC accumulation and lower levels of hepatic ^{18}F-DFA accumulation compared to vehicle-treated mice (**Fig. 1B, C; Fig. S1**).

Consistent with a functional role for the immune system in ConA-induced hepatitis (*9*), liver sections from immunocompromised NOD *scid* gamma (NSG) mice treated with ConA were indistinguishable histologically or immunohistochemically from liver sections of control mice (**Fig. S2A**). No difference in hepatic ^{18}F-FDG, ^{18}F-FAC, or ^{18}F-DFA accumulation was observed between vehicle- and ConA-treated immunocompromised mice (**Fig. S2B, C; Fig. S1**), indicating that the changes we observed in hepatic tracer accumulation in the immunocompetent mice are due to the ConA-induced hepatitis and not unrelated effects of the ConA treatment.

Hepatic infiltrating CD4 T cells are the major source of increased hepatic ^{18}F-FAC accumulation in ConA-induced autoimmune hepatitis. To better understand why hepatic ^{18}F-FDG, ^{18}F-FAC, and ^{18}F-DFA accumulation is affected in ConA-induced autoimmune hepatitis, we studied the system at a cellular level. The cellular accumulation of ^{18}F-FDG, ^{18}F-FAC, and ^{18}F-DFA are regulated by specific proteins (*18*,*35*,*36*), and changes in the levels of these proteins in the liver could in part explain changes in hepatic radiotracer accumulation. Expression and membrane localization of the facilitative glucose transporter GLUT1 is a major determinant of glucose consumption in activated lymphocytes, dCK regulates the cellular accumulation of ^{18}F-FAC, and RBKS is a key enzyme in the ribose salvage pathway that ^{18}F-DFA measures (*36*–*38*).

Liver sections from ConA-treated mice immunostained for GLUT1 showed high levels of membrane-localized GLUT1 in hepatic infiltrating leukocytes as well as increased GLUT1 membrane expression in leukocyte-proximal liver sinusoidal endothelial cells (**Fig. 2A**). RBKS protein levels were absent from hepatic infiltrating leukocytes but present at high levels in liver hepatocytes (**Fig. 2A**). Hepatic infiltrating leukocytes in ConA-treated mice expressed high dCK protein levels, and hepatocyte dCK levels were similar between vehicle and ConA-treated mouse liver sections (**Fig. 2A**). GLUT1, RBKS, and dCK protein levels were unaffected in the livers of ConA-treated compared to vehicle-treated immunocompromised mice (**Fig. S3**).

Autoradiography results of liver sections from vehicle- or ConA-treated mice injected with ^{18}F-FDG, ^{18}F-FAC, or ^{18}F-DFA were co-registered with images of these same sections stained with H&E. Areas of increased ^{18}F-FDG and ^{18}F-FAC accumulation, measured by autoradiography, were coincident with areas of significant leukocyte infiltration (**Fig. 2B**), suggesting that hepatic infiltrating leukocytes are a major source of the increased hepatic ^{18}F-FDG and ^{18}F-FAC accumulation identified in ConA-treated mice.

Regions of increased autoradiographic signal in the ConA-treated mice injected with ^{18}F-FDG were 2.8-fold larger than in the ConA-treated mice injected with ^{18}F-FAC ($p < 0.0001$). This may indicate greater specificity of ^{18}F-FAC than ^{18}F-FDG for hepatic infiltrating leukocytes, which is consistent with the immunohistochemistry results (**Fig. 2A**). ^{18}F-DFA accumulation was decreased throughout the liver in ConA-treated mice and not coincident with regions of significant leukocyte infiltration (**Fig. 2B**), consistent with decreased ribose salvage activity in hepatocytes throughout the liver. This data suggests that in ConA-treated mice, hepatic infiltrating leukocytes consume high levels of ^{18}F-FAC, hepatic infiltration leukocytes and nearby liver sinusoidal endothelial cells consume high levels of ^{18}F-FDG, and inflamed hepatocytes decrease their ^{18}F-DFA accumulation.

Given the potential specificity of ^{18}F-FAC for hepatic infiltrating leukocytes, the further selectivity of ^{18}F-FAC for specific leukocyte populations was analyzed. A previous study demonstrated that during immune-mediated tumor rejection, ^{18}F-FAC preferentially accumulated in adaptive immune cells (*24*). Our immunohistochemistry data suggests that CD4, CD8, B220, and CD11b positive leukocytes all infiltrate into the liver in the ConA-treated mice (**Fig. 1A**). CD4-, CD8-, B220-, and CD11b-positive cells were isolated from the liver of ConA-treated mice and incubated with ^{3}H-deoxycytidine to measure deoxynucleoside salvage activity. Per cell, CD4 and CD8 T cells consumed approximately 4-fold more deoxycytidine than B220 or CD11b cells (**Fig. 2C**), and CD4 T cells were present in higher numbers than CD8 T cells in ConA-treated livers (**Fig. 1A**). Collectively this data suggests that increased hepatic ^{18}F-FAC accumulation predominantly measures infiltrating CD4 cells in the livers of ConA-treated mice.

Hepatic accumulation of ^{18}F-FDG and ^{18}F-DFA but not ^{18}F-FAC are affected by viral hepatitis. Autoimmune hepatitis is one, but not the only, condition characterized by immune cell infiltration into the liver. Histologically, viral hepatitis closely resembles

autoimmune hepatitis. We studied the behavior of ^{18}F-FDG, ^{18}F-FAC, and ^{18}F-DFA in a model of viral hepatitis. Viral hepatitis was induced by treating mice with a replication-defective GFP-expressing adenovirus. Immunocompromised NSG mice were used to control for non-immune related effects of the adenoviral treatment on radiotracer accumulation. Mice treated with the adenovirus mount a robust immune attack on the liver within two weeks of treatment that persists through eight weeks before clearing by 12 weeks, leaving only histiocytes as evidence of the antecedent inflammation (**Fig. 3A**). Within the periportal leukocyte infiltrates, a significant proportion of the cells consisted of CD4 T cells and CD11b-positive innate immune cells while a smaller proportion of the cells consisted of B220-positive B cells and CD8-positive T cells (36 ± 2%, 47 ± 4%, 10 ± 2%, 11 ± 2%, respectively). A smaller fraction of the infiltrating leukocytes was Ki67 positive compared to the autoimmune hepatitis model (37 ± 3% for this model versus 67 ± 4% for the autoimmune hepatitis model; **Fig. 1A, 3A**). At the level of histology and immunohistochemistry, livers of the immunocompromised mice were largely unaffected by the viral treatment (**Fig. S4A**).

Similar to results obtained in the autoimmune hepatitis model, viral hepatitis induced a significant increase in hepatic ^{18}F-FDG accumulation that returned to pre-treatment levels after the hepatitis resolved (**Fig. 3B, C; Fig. S5**). Viral hepatitis also decreased hepatic ^{18}F-DFA accumulation, which returned to higher than baseline levels at 12 weeks post-treatment (**Fig. 3B, C; Fig. S5**). We speculate that hepatic ^{18}F-DFA accumulation is elevated at 12 weeks post-treatment because of a compensatory response of the liver hepatocytes to the prior decrease in hepatic ^{18}F-DFA accumulation. In contrast to the results from the autoimmune hepatitis model (**Fig. 1B, C**), hepatic ^{18}F-FAC accumulation was unaffected at any time point throughout the induction and clearance of the viral hepatitis (**Fig. 3B, C; Fig. S5**). No change in hepatic ^{18}F-FDG, ^{18}F-DFA, or ^{18}F-FAC accumulation was identified in immunocompromised mice treated with

adenovirus, suggesting that the above results required immune activation (**Fig. S4B, C; Fig. S5**).

Changes in hepatic ^{18}F-FAC accumulation can be used to monitor immunosuppressive drug treatments in a mouse model of autoimmune hepatitis. One potential application for a PET strategy that can quantify hepatic infiltrating CD4 and CD8 T lymphocytes is monitoring the response of these cells to immunosuppressive therapies, similar to the role of PET in other fields including oncology (*39*). Studies suggest and we found that pretreatment of mice with the immunosuppressive drug dexamethasone can block ConA-induced autoimmune hepatitis (**Fig. 4A**) (*9*). Mice treated with dexamethasone 18 and 1 hour prior to treatment with ConA had significantly lower levels of hepatic ^{18}F-FAC accumulation than mice treated with ConA and vehicle (**Fig. 4B, C**). This suggests that PET imaging with ^{18}F-FAC could be used as a biomarker for immunomodulatory therapies developed to treat autoimmune hepatitis.

Hepatic infiltrating leukocytes in patients with autoimmune hepatitis express dCK. Our data suggest that ^{18}F-FAC may selectively image CD4 and CD8 T cells during autoimmune hepatitis. Whether this is true in humans remains to be determined and is the basis for future studies. To assess deoxynucleoside salvage activity in hepatic infiltrating leukocytes in human patients with autoimmune hepatitis, we immunostained tissue sections from biopsies of patients suffering from autoimmune hepatitis for dCK. Hepatic infiltrating leukocytes in these liver sections stained strongly for dCK (**Fig. 5**). This provides early evidence that PET tracers that measure dCK activity could potentially be used to quantify hepatic infiltrating lymphocytes in humans with autoimmune hepatitis.

Discussion

In our studies, ^{18}F-FAC selectively accumulates in the autoimmune but not viral hepatitis model. Hepatic ^{18}F-FDG and ^{18}F-DFA accumulation were affected by similar amounts in the autoimmune and viral hepatitis models, suggesting that the difference in ^{18}F-FAC accumulation between the two models is not due solely to differences in the magnitude of the immune response. Determining the precise mechanism for the selectivity of ^{18}F-FAC for autoimmune over viral hepatitis is beyond the scope of this work. However previous studies suggest a strong correlation between ^{18}F-FAC accumulation and cell cycle in immune cells (*24*). The ConA-induced autoimmune hepatitis model has faster kinetics than the viral hepatitis model. ConA induces autoimmune hepatitis within 24 hours of injection that begins to clear by 48 hours. The viral hepatitis is induced within 2 weeks and takes 12 weeks to clear. Consistent with these kinetics, a higher percentage of hepatic infiltrating leukocyte are positive for the cellular proliferation marker Ki67 in the ConA-induced autoimmune hepatitis model than in the viral hepatitis model (67 ± 4% versus 37 ± 3%, respectively; **Fig. 1A, 3A**). Additionally we show high deoxynucleoside salvage activity in CD4 T cells in the autoimmune hepatitis model, and this model has a higher percent of CD4 T cells among the hepatic infiltrating leukocytes than does the viral hepatitis model (64 ± 2% versus 36 ± 2%, respectively). This may suggest that ^{18}F-FAC accumulates in hepatic infiltrating lymphocytes in the ConA-induced autoimmune hepatitis model due to a greater percent of CD4 cells and greater cell proliferation among the infiltrating immune cells in this model.

We identify that hepatic ribose salvage activity is decreased uniformly throughout liver hepatocytes in both the autoimmune and viral hepatitis models and is not localized to areas of significant leukocyte infiltration. Little is known about the regulation of ribose salvage activity. However the fact that ribose salvage is affected in hepatocytes adjacent to and distant from the infiltration immune cells suggests a potential role for cytokines in

this process. Previous studies report that during ConA-induced autoimmune hepatitis, plasma protein and liver mRNA levels of cytokines including TNF, IFN(gamma), IL-2, IL-4, IL-6, IL-10, and IL-12 are all elevated (*40*). Whether cytokines regulate ribose salvage activity in this model remains to be determined.

Our studies suggest that deoxynucleoside salvage activity in the liver, measured by ^{18}F-FAC accumulation, is higher in a mouse model of autoimmune hepatitis than control mice. dCK is a rate limiting enzyme for deoxynucleoside salvage (*36*). The precise role of deoxynucleoside salvage in T cell activation is not well-described, but genetic inactivation of dCK in mice blocks lymphocyte development and leads to significantly lower lymphocyte numbers (*36*). Recently small molecule inhibitors of dCK have been developed (*41*). While further studies are required, our results may suggest new therapeutic opportunities for targeting dCK in the context of autoimmune hepatitis.

Implications for human studies.

Diagnosing autoimmune hepatitis and hepatic allograft rejection and monitoring therapeutic responses in these diseases remains a challenge (*42–44*). In routine clinical practice, autoimmune hepatitis is diagnosed through descriptive criteria with consideration for features such as liver histology and serum biochemistries. A semi-quantitative scoring system used in clinical trials that attributes positive or negative points to the presence or absence of alterations in liver histology, serum biochemistry, and serum autoantibodies improves on the descriptive criteria (*1*). Similarly, hepatic allograft rejection is diagnosed through a combination of liver biochemistry measurements and histological features (*2*). All of these approaches depend on interpreting the results of a liver biopsy, which can be subject to significant sampling and reader error and are not without risk (*14–17*). We hypothesize that PET imaging with ^{18}F-FAC (or ^{18}F-FAC derivatives) could provide a tomographic, whole organ, quantitative assessment of activated hepatic infiltrating

lymphocytes in these diseases and could complement biopsies. ^{18}F-DFA PET could provide the same with respect to the presence of inflamed hepatocytes.

Autoimmune hepatitis and hepatic allograft rejection are treated with immunosuppressive drugs (*1*,*2*). These therapies are often effective but have narrow therapeutic windows, significant side effects, and high patient-to-patient variability in their pharmacokinetics and pharmacodynamics (*45*,*46*). Without a method for quantifying activated immune cells in the liver, identifying the correct dose of an immunosuppressive drug for an individual patient that blocks immune attack on the liver while limiting unwanted side effects remains a significant clinical challenge (*47*). The ability to directly and quantitatively measure hepatic infiltrating lymphocytes – a desired target of these immunomodulatory drugs – could serve as a valuable biomarker for assessing efficacy. Here we show in a mouse model that ^{18}F-FAC PET can quantitatively assess hepatic infiltrating lymphocytes and can be used to monitor the efficacy of an immunomodulatory drug.

The most prevalent hepatitis-inducing viruses in humans are Hepatitis B and C. These diseases can occur as acute infections that resolve or can persist as chronic infections (*48*). Insofar as the adenovirus infection in mice resolves, it models an acute rather than a chronic infection. The lack of any effect on hepatic radiotracer accumulation in the adenovirus-treated immunocompromised mice suggests that the effects identified in the adenovirus-treated immunocompetent mice are solely due to immune attack on the liver and not the adenovirus infection by itself. Chronic hepatitis infections are characterized by exhausted and impaired immune cell responses to the virus, an immunological state associated with decreased glucose consumption (*48*,*49*). We would have to study a chronic hepatitis model to understand the behavior of the radiotracers during a chronic infection. However, we can speculate that the differences we identify

here in hepatic ^{18}F-FDG and ^{18}F-DFA accumulation during the adenoviral infection would likely be muted during a chronic infection.

In a recent study, we showed that ribose salvage activity, the biochemical pathway measured by ^{18}F-DFA, is similar between mouse and human hepatocytes in culture and when engrafted into a mouse liver (*20*). This suggests that the ^{18}F-DFA imaging results presented here may be translatable into human studies.

^{18}F-FAC images dCK activity in mice but is subject to deamination by the enzyme cytidine deaminase (CDA) (*50*). CDA activity is higher in most human than mouse tissue, and ^{18}F-FAC accumulation in lymphoid organs such as the spleen is lower in humans than mice (*24*,*51*,*52*). ^{18}F-FAC accumulation is also low in the human liver (*52*). The PET radiotracer 2-chloro-2'-deoxy-2'-[^{18}F]fluoro-9-D-arabinofuranosyl-adenine (^{18}F-CFA) is a substrate for dCK and resistant to deamination by CDA (*53*). ^{18}F-CFA accumulates at high levels in lymphoid organs in humans but also at high levels in the healthy human liver (*54*). High ^{18}F-CFA accumulation in the healthy liver would disfavor its use for imaging lymphocytes in the human liver. However whether activated human CD4 and CD8 T cells could accumulate sufficient ^{18}F-FAC in the setting of high intracellular and peripheral CDA activity to produce a PET image remains to be determined.

Conclusions

Our results suggest that PET imaging could potentially provide a quantitative, non-invasive method for monitoring hepatocytes and hepatic infiltrating T cells during autoimmune hepatitis and in response to therapy. Previous studies suggest that ^{18}F-FAC can be used visualize a mouse model of systemic autoimmunity and colitis (*23*,*26*). The value of this with respect to treatment would be in directly assessing the targets of disease modifying therapies. Collectively these studies begin to suggest a potential role for ^{18}F-

FAC PET and PET tracers with organ specific accumulation to visualize and quantify the development and treatment of autoimmune diseases.

Disclosures

PMC and ONW are inventors on a patent, held by the Regents of the University of California, that describes the ^{18}F-DFA radiotracer. ONW is an inventor on a patent, held by the Regents of the University of California, that describes the ^{18}F-FAC radiotracer.

Acknowledgements

We thank the UCLA Translational Pathology Core Laboratory, the Crump Preclinical Imaging Technology Center, and the Crump Cyclotron and Radiochemistry Technology Center for assisting in these studies. We thank Ralph and Marjorie Crump for their gift to the UCLA Crump Institute for Molecular Imaging. This work was supported by the NIH Grant #R21AI119916 (to P.M.C.), the Parker Institute for Cancer Immunotherapy (PICI) Grant #20163828 (to O.N.W.), and the Broad Stem Cell Research Center at UCLA.

References

1. Manns MP, Czaja AJ, Gorham JD, et al. Diagnosis and management of autoimmune hepatitis. *Hepatology*. 2010;51:2193-2213.

2. Batts KP. Acute and chronic hepatic allograft rejection: pathology and classification. *Liver Transpl Surg*. 1999;5:S21-29.

3. Rosen HR. Transplantation immunology: what the clinician needs to know for immunotherapy. *Gastroenterology*. 2008;134:1789-1801.

4. Markmann JF, Markowitz JS, Yersiz H, et al. Long-term survival after retransplantation of the liver. *Ann Surg*. 1997;226:408-418; discussion 418-420.

5. Senaldi G, Portmann B, Mowat AP, Mieli-Vergani G, Vergani D. Immunohistochemical features of the portal tract mononuclear cell infiltrate in chronic aggressive hepatitis. *Arch Dis Child*. 1992;67:1447-1453.

6. McCaughan GW, Davies JS, Waugh JA, et al. A quantitative analysis of T lymphocyte populations in human liver allografts undergoing rejection: the use of monoclonal antibodies and double immunolabeling. *Hepatology*. 1990;12:1305-1313.

7. Li W, Lu L, Wang Z, et al. Il-12 antagonism enhances apoptotic death of T cells within hepatic allografts from Flt3 ligand-treated donors and promotes graft acceptance. *J Immunol*. 2001;166:5619-5628.

8. Qian S, Lu L, Fu F, et al. Apoptosis within spontaneously accepted mouse liver allografts: evidence for deletion of cytotoxic T cells and implications for tolerance induction. *J Immunol*. 1997;158:4654-4661.

9. Tiegs G, Hentschel J, Wendel A. A T cell-dependent experimental liver injury in mice inducible by concanavalin A. *J Clin Invest*. 1992;90:196-203.

10. Czaja AJ, Wolf AM, Baggenstoss AH. Laboratory assessment of severe chronic active liver disease during and after corticosteroid therapy: correlation of serum transaminase and gamma globulin levels with histologic features. *Gastroenterology*. 1981;80:687-692.

11. Czaja AJ, Ludwig J, Baggenstoss AH, Wolf A. Corticosteroid-treated chronic active hepatitis in remission: uncertain prognosis of chronic persistent hepatitis. *N Engl J Med*. 1981;304:5-9.

12. Grunwald D, Kothari D, Malik R. Noninvasive markers in the assessment and management of autoimmune liver diseases. *Eur J Gastroenterol Hepatol*. 2014;26:1065-1072.

13. Rodrigo E, López-Hoyos M, Corral M, et al. ImmuKnow as a diagnostic tool for predicting infection and acute rejection in adult liver transplant recipients: a systematic review and meta-analysis. *Liver Transpl*. 2012;18:1245-1253.

14. Bubak ME, Porayko MK, Krom RA, Wiesner RH. Complications of liver biopsy in liver transplant patients: increased sepsis associated with choledochojejunostomy. *Hepatology*. 1991;14:1063-1065.

15. Regev A, Berho M, Jeffers LJ, et al. Sampling error and intraobserver variation in liver biopsy in patients with chronic HCV infection. *Am J Gastroenterol*. 2002;97:2614-2618.

16. Aran PP, Bissel MG, Whitington PF, Bostwick DG, Adamac T, Baker AL. Diagnosis of hepatic allograft rejection: role of liver biopsy. *Clin Transplant*. 1993;7:475-481.

17. Coffin CS, Burak KW, Hart J, Gao Z. The impact of pathologist experience on liver transplant biopsy interpretation. *Mod Pathol*. 2006;19:832-838.

18. Clark PM, Flores G, Evdokimov NM, et al. Positron emission tomography probe demonstrates a striking concentration of ribose salvage in the liver. *Proc Natl Acad Sci U S A*. 2014;111:E2866-2874.

19. Evdokimov NM, Clark PM, Flores G, et al. Development of 2-Deoxy-2-[(18)F]fluororibose for Positron Emission Tomography Imaging Liver Function in Vivo. *J Med Chem*. 2015;58:5538-5547.

20. Salas JR, Chen BY, Wong A, et al. Non-invasive imaging of drug-induced liver injury with 18F-DFA PET. *J Nucl Med*. March 2018.

21. Laing RE, Nair-Gill E, Witte ON, Radu CG. Visualizing cancer and immune cell function with metabolic positron emission tomography. *Curr Opin Genet Dev*. 2010;20:100-105.

22. Radu CG, Shu CJ, Shelly SM, Phelps ME, Witte ON. Positron emission tomography with computed tomography imaging of neuroinflammation in experimental autoimmune encephalomyelitis. *Proc Natl Acad Sci U S A*. 2007;104:1937-1942.

23. Radu CG, Shu CJ, Nair-Gill E, et al. Molecular imaging of lymphoid organs and immune activation by positron emission tomography with a new [18F]-labeled 2'-deoxycytidine analog. *Nat Med*. 2008;14:783-788.

24. Nair-Gill E, Wiltzius SM, Wei XX, et al. PET probes for distinct metabolic pathways have different cell specificities during immune responses in mice. *J Clin Invest*. 2010;120:2005-2015.

25. Brewer S, McPherson M, Fujiwara D, et al. Molecular imaging of murine intestinal inflammation with 2-deoxy-2-[18F]fluoro-D-glucose and positron emission tomography. *Gastroenterology*. 2008;135:744-755.

26. Brewer S, Nair-Gill E, Wei B, et al. Epithelial uptake of [18F]1-(2'-deoxy-2'-arabinofuranosyl) cytosine indicates intestinal inflammation in mice. *Gastroenterology*. 2010;138:1266-1275.

27. de Paula Faria D, Vlaming MLH, Copray SCVM, et al. PET imaging of disease progression and treatment effects in the experimental autoimmune encephalomyelitis rat model. *J Nucl Med*. 2014;55:1330-1335.

28. Maya Y, Werner RA, Schütz C, et al. 11C-Methionine PET of Myocardial Inflammation in a Rat Model of Experimental Autoimmune Myocarditis. *J Nucl Med*. 2016;57:1985-1990.

29. Terry SYA, Koenders MI, Franssen GM, et al. Monitoring Therapy Response of Experimental Arthritis with Radiolabeled Tracers Targeting Fibroblasts, Macrophages, or Integrin αvβ3. *J Nucl Med*. 2016;57:467-472.

30. Ishimori T, Saga T, Mamede M, et al. Increased (18)F-FDG uptake in a model of inflammation: concanavalin A-mediated lymphocyte activation. *J Nucl Med*. 2002;43:658-663.

31. Tsuji AB, Morita M, Li X-K, et al. 18F-FDG PET for semiquantitative evaluation of acute allograft rejection and immunosuppressive therapy efficacy in rat models of liver transplantation. *J Nucl Med*. 2009;50:827-830.

32. Collins J, Waldmann CM, Drake C, et al. Production of diverse PET probes with limited resources: 24 18F-labeled compounds prepared with a single radiosynthesizer. *Proc Natl Acad Sci U S A*. 2017;114:11309-11314.

33. Blom KG, Qazi MR, Matos JBN, Nelson BD, DePierre JW, Abedi-Valugerdi M. Isolation of murine intrahepatic immune cells employing a modified procedure for mechanical disruption and functional characterization of the B, T and natural killer T cells obtained. *Clin Exp Immunol*. 2009;155:320-329.

34. Gantner F, Leist M, Lohse AW, Germann PG, Tiegs G. Concanavalin A-induced T-cell-mediated hepatic injury in mice: the role of tumor necrosis factor. *Hepatology*. 1995;21:190-198.

35. Phelps ME. Positron emission tomography provides molecular imaging of biological processes. *Proc Natl Acad Sci U S A*. 2000;97:9226-9233.

36. Toy G, Austin WR, Liao H-I, et al. Requirement for deoxycytidine kinase in T and B lymphocyte development. *Proc Natl Acad Sci U S A*. 2010;107:5551-5556.

37. Jacobs SR, Herman CE, Maciver NJ, et al. Glucose uptake is limiting in T cell activation and requires CD28-mediated Akt-dependent and independent pathways. *J Immunol*. 2008;180:4476-4486.

38. Agranoff BW, Brady RO. Purification and properties of calf liver ribokinase. *J Biol Chem*. 1956;219:221-229.

39. Clark PM, Ebiana VA, Gosa L, Cloughesy TF, Nathanson DA. Harnessing Preclinical Molecular Imaging to Inform Advances in Personalized Cancer Medicine. *J Nucl Med*. 2017;58:689-696.

40. Sass G, Heinlein S, Agli A, Bang R, Schümann J, Tiegs G. Cytokine expression in three mouse models of experimental hepatitis. *Cytokine*. 2002;19:115-120.

41. Murphy JM, Armijo AL, Nomme J, et al. Development of new deoxycytidine kinase inhibitors and noninvasive in vivo evaluation using positron emission tomography. *J Med Chem*. 2013;56:6696-6708.

42. Czaja AJ. Challenges in the diagnosis and management of autoimmune hepatitis. *Can J Gastroenterol*. 2013;27:531-539.

43. Dyson JK, Webb G, Hirschfield GM, et al. Unmet clinical need in autoimmune liver diseases. *J Hepatol*. 2015;62:208-218.

44. Staatz CE, Tett SE. Clinical pharmacokinetics and pharmacodynamics of tacrolimus in solid organ transplantation. *Clin Pharmacokinet*. 2004;43:623-653.

45. Jusko WJ, Piekoszewski W, Klintmalm GB, et al. Pharmacokinetics of tacrolimus in liver transplant patients. *Clin Pharmacol Ther*. 1995;57:281-290.

46. Lampen A, Christians U, Guengerich FP, et al. Metabolism of the immunosuppressant tacrolimus in the small intestine: cytochrome P450, drug interactions, and interindividual variability. *Drug Metab Dispos*. 1995;23:1315-1324.

47. Zarrinpar A, Lee D-K, Silva A, et al. Individualizing liver transplant immunosuppression using a phenotypic personalized medicine platform. *Sci Transl Med*. 2016;8:333ra49.

48. Shin E-C, Sung PS, Park S-H. Immune responses and immunopathology in acute and chronic viral hepatitis. *Nat Rev Immunol*. 2016;16:509-523.

49. Bengsch B, Johnson AL, Kurachi M, et al. Bioenergetic Insufficiencies Due to Metabolic Alterations Regulated by the Inhibitory Receptor PD-1 Are an Early Driver of CD8(+) T Cell Exhaustion. *Immunity*. 2016;45:358-373.

50. Shu CJ, Campbell DO, Lee JT, et al. Novel PET probes specific for deoxycytidine kinase. *J Nucl Med*. 2010;51:1092-1098.

51. Ho DH. Distribution of kinase and deaminase of 1-beta-D-arabinofuranosylcytosine in tissues of man and mouse. *Cancer Res*. 1973;33:2816-2820.

52. Schwarzenberg J, Radu CG, Benz M, et al. Human biodistribution and radiation dosimetry of novel PET probes targeting the deoxyribonucleoside salvage pathway. *Eur J Nucl Med Mol Imaging*. 2011;38:711-721.

53. Kim W, Le TM, Wei L, et al. [18F]CFA as a clinically translatable probe for PET imaging of deoxycytidine kinase activity. *Proc Natl Acad Sci U S A*. 2016;113:4027-4032.

54. Barrio MJ, Spick C, Radu CG, et al. Human Biodistribution and Radiation Dosimetry of 18F-Clofarabine, a PET Probe Targeting the Deoxyribonucleoside Salvage Pathway. *J Nucl Med*. 2017;58:374-378.

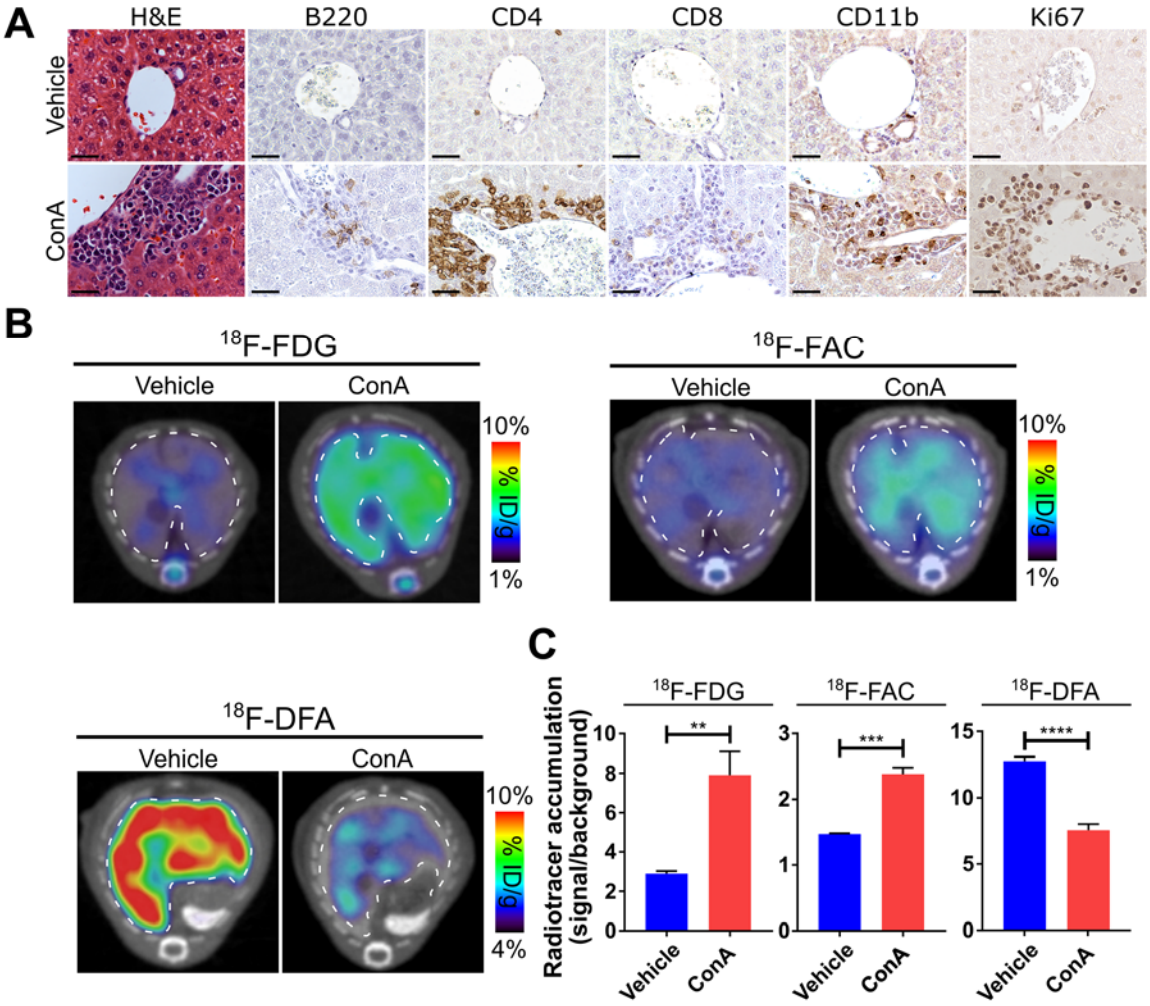

Figure 1: Hepatic ^{18}F-FDG, ^{18}F-FAC, and ^{18}F-DFA accumulation are affected in a mouse model of autoimmune hepatitis. (A) Histochemical and immunohistochemical analyses of liver sections from vehicle- and ConA-treated mice. Scale bars represent 50 microns. Transverse PET/CT images (B) and quantification (C) of vehicle- and ConA-treated mice injected with ^{18}F-FDG, ^{18}F-FAC, and ^{18F}DFA. Livers are outlined in a white dotted line. Quantification represents radiotracer accumulation in the liver normalized to a background organ. **: $P < 0.01$; ***: $P < 0.001$; ****: $P < 0.0001$.

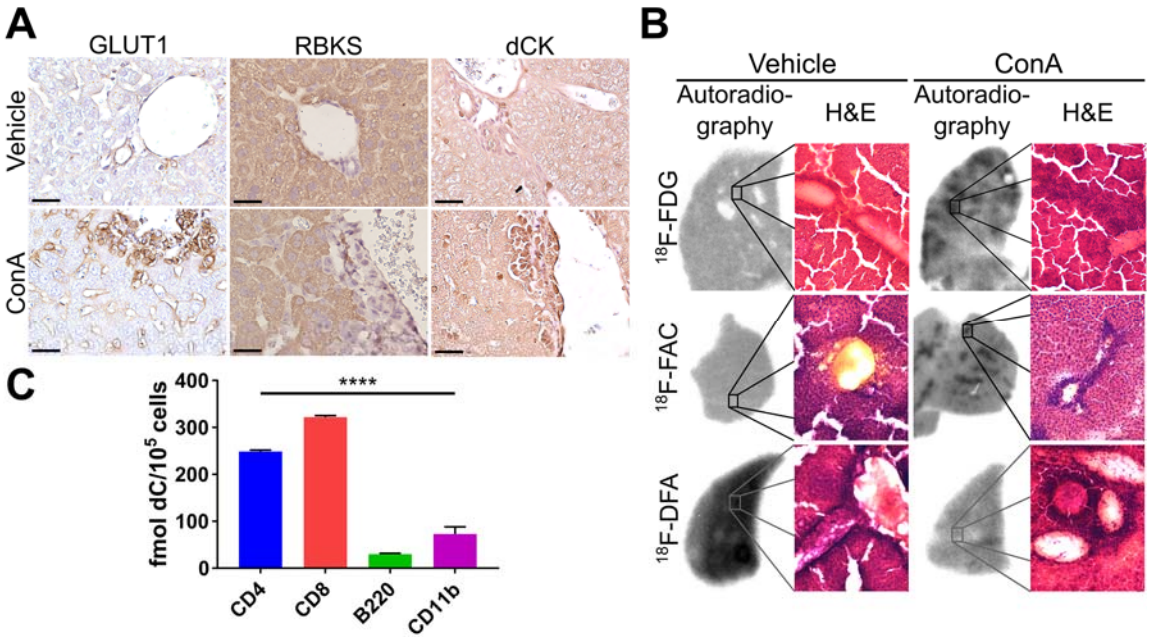

Figure 2: ^{18}F-FDG and ^{18}F-FAC measure hepatic infiltrating leukocytes, and ^{18}F-DFA measures hepatocyte inflammation. (A) GLUT1, RBKS, and dCK immunostained vehicle- and ConA-treated mouse liver sections. Scale bars represent 50 microns. (B) Autoradiographic and histological analyses of liver sections from vehicle- and ConA-treated mice injected with ^{18}F-FDG, ^{18}F-FAC, or ^{18}F-DFA. (C) *Ex vivo* accumulation of deoxycytidine in sorted leukocytes from the livers of ConAtreated mice. ****: $P < 0.0001$.

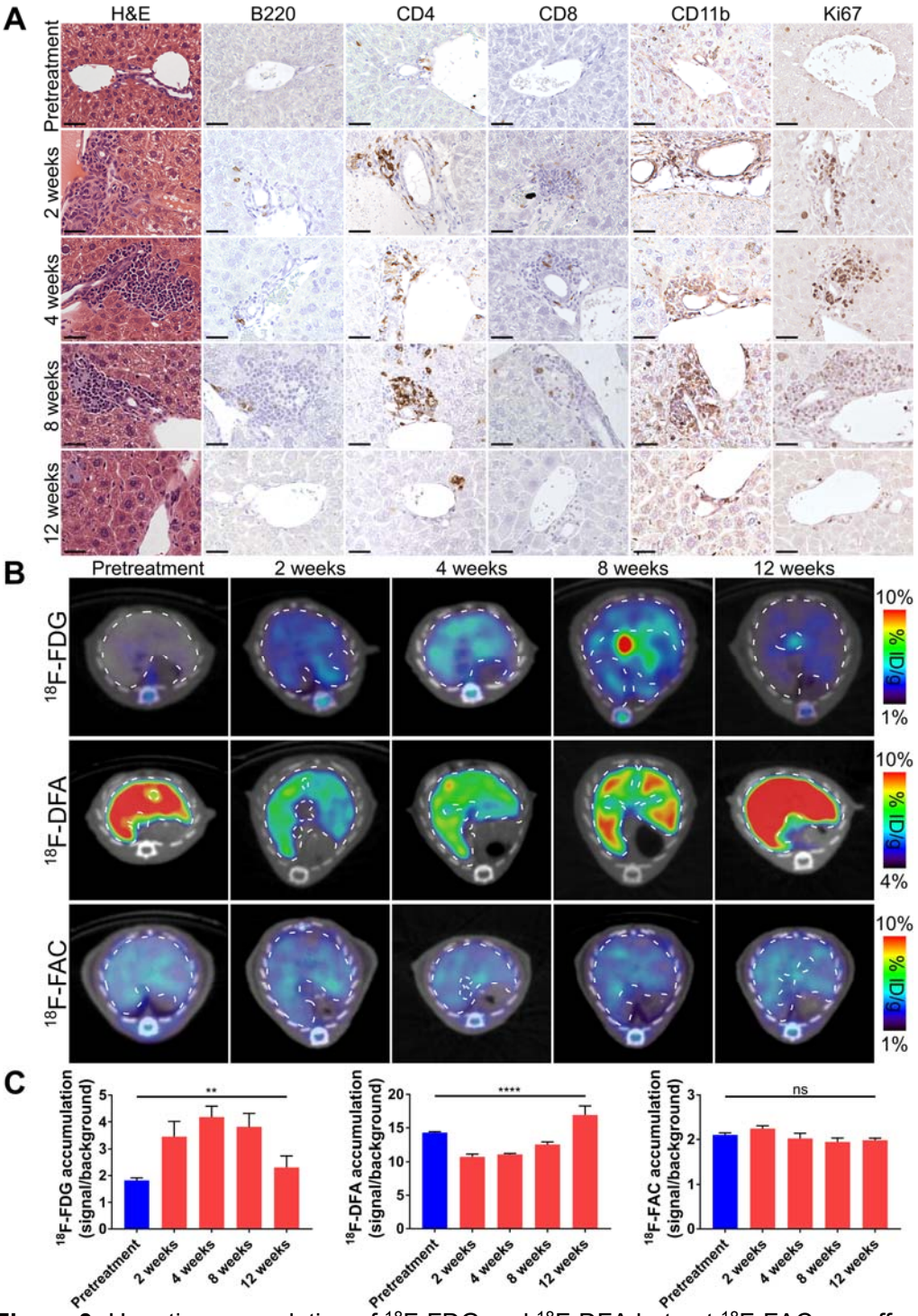

Figure 3: Hepatic accumulation of ^{18}F-FDG and ^{18}F-DFA but not ^{18}F-FAC are affected in a mouse model of viral hepatitis. (A) Histochemical and immunohistochemical analyses of liver sections from pretreatment and adenovirus-treated mice. Scale bar represents 50 microns. Transverse PET/CT images (B) and quantification (C) of pretreatment and adenovirus-treated mice injected with ^{18}F-FDG, ^{18}F-DFA, and ^{18}F-FAC. Quantification represents radiotracer accumulation in the liver normalized to a background organ. **: $P < 0.01$; ****: $P < 0.0001$; ns: not significant.

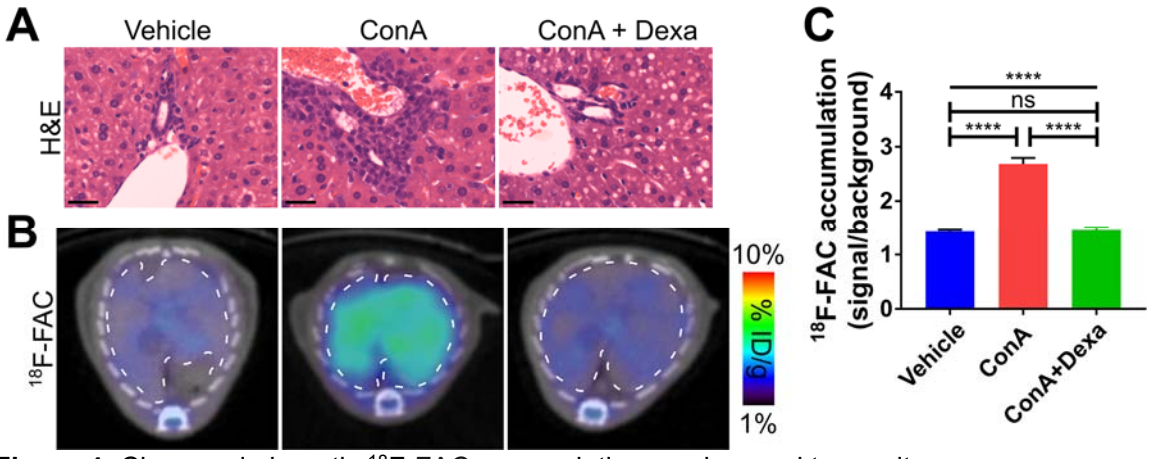

Figure 4: Changes in hepatic ^{18}F-FAC accumulation can be used to monitor immunosuppressive drug treatments in a mouse model of autoimmune hepatitis. (A) Representative H&E-stained liver sections of mice treated with vehicle, ConA, or ConA and dexamethasone (Dexa). Scale bars represent 50 microns. (B) Transverse PET/CT images of hepatic ^{18}F-FAC accumulation in mice treated with vehicle, ConA, or ConA and Dexa. (C) Quantification of hepatic ^{18}F-FAC accumulation in mice treated with vehicle, ConA, or ConA and Dexa. Quantification represents radiotracer accumulation in the liver normalized to a background organ. ****: $P < 0.0001$; ns: not significant.

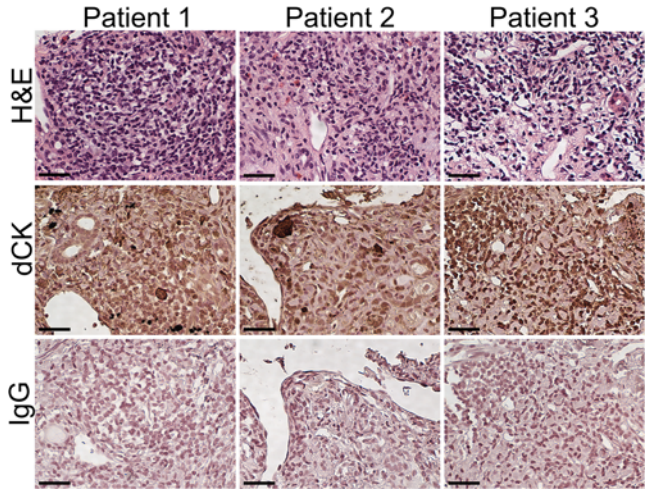

Figure 5: Hepatic infiltrating leukocytes in patients with autoimmune hepatitis express dCK. Histochemical and immunohistochemical analyses of liver biopsies from patients with autoimmune hepatitis. Scale bar represents 50 microns.

Supplemental information

^{18}F-FAC PET selectively images hepatic infiltrating CD4 and CD8 T cells in a mouse model of autoimmune hepatitis

Jessica R. Salas[1,2], Bao Ying Chen[1,2], Alicia Wong[1,2], Donghui Cheng[3], John S. Van Arnam[5], Owen N. Witte[1,3,4], Peter M. Clark[1,2,3,‡]

[1] Department of Molecular and Medical Pharmacology, [2] Crump Institute for Molecular Imaging, [3] Eli and Edythe Broad Center of Regenerative Medicine and Stem Cell Research, [4] Department of Microbiology, Immunology, and Molecular Genetics, University of California, Los Angeles, CA 90095. [5] Department of Pathology and Laboratory Medicine, University of Pennsylvania, Philadelphia, CA 19104

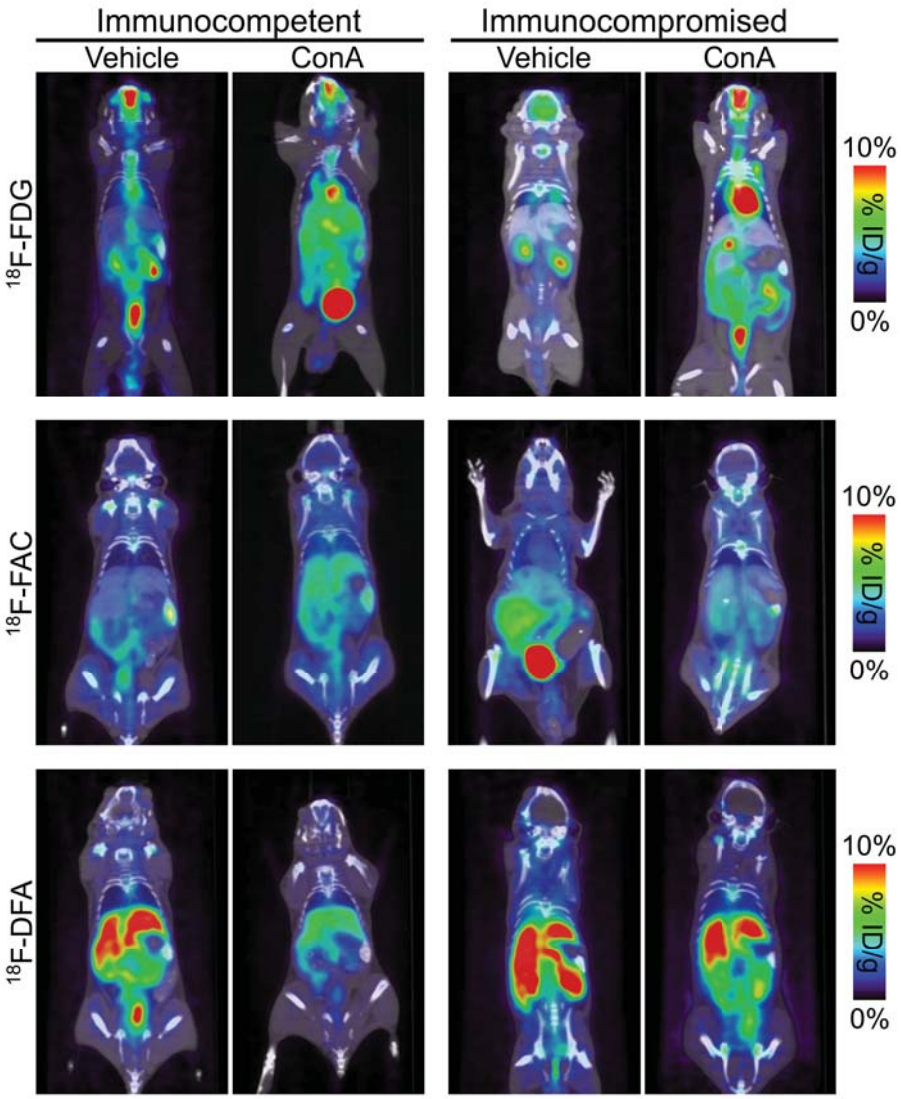

Figure S1: ^{18}F-FDG, ^{18}F-FAC, and ^{18}F-DFA accumulation in mice treated with ConA. Representative coronal sections of vehicle- and ConA-treated immunocompetent or immunocompromised mice injected with ^{18}F-FDG, ^{18}F-FAC, and ^{18}F-DFA.

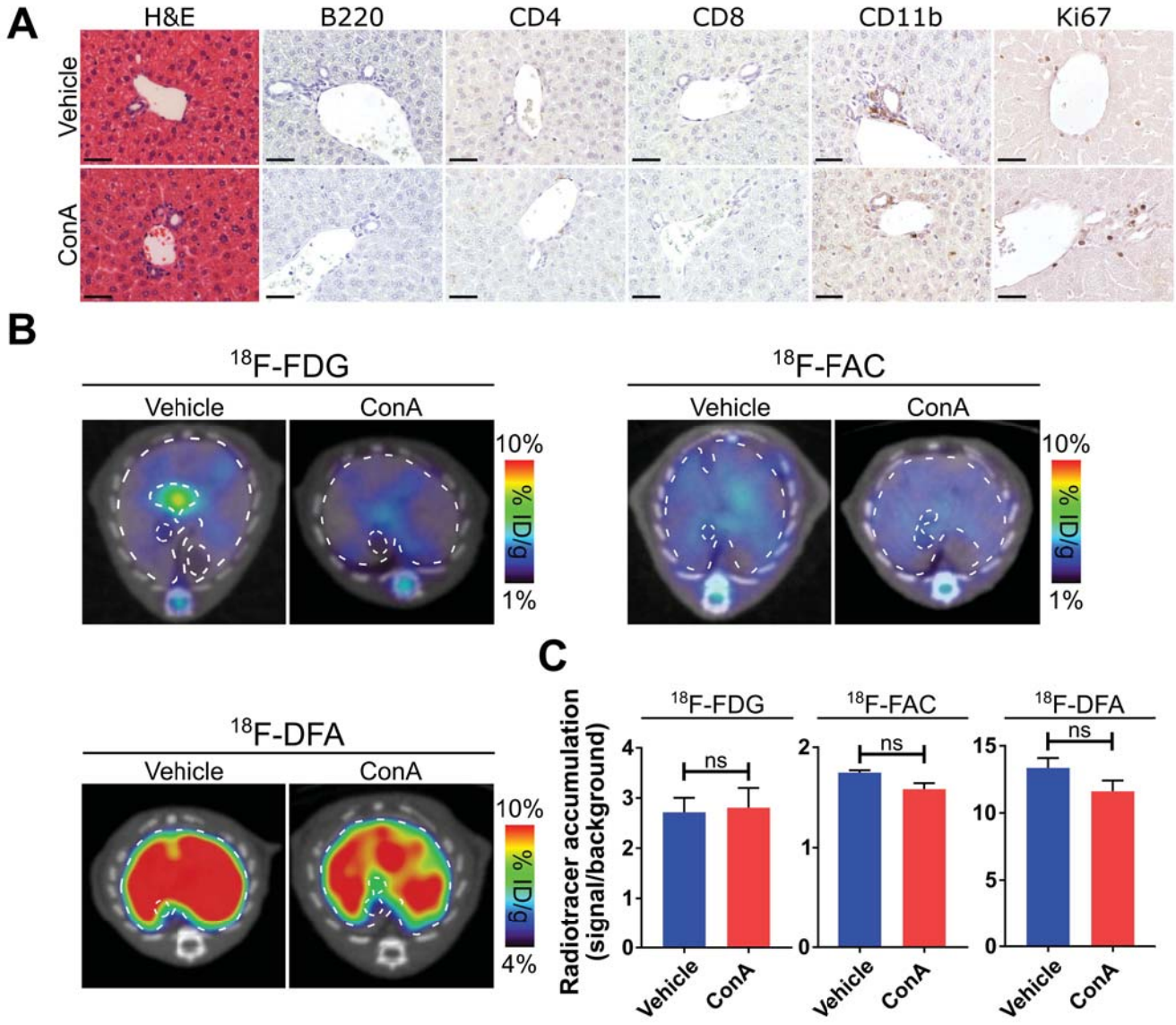

Figure S2: Hepatic ^{18}F-FDG, ^{18}F-FAC, and ^{18}F-DFA accumulation are unaffected in immunocompromised mice treated with ConA. (A) Histochemical and immunohistochemical analyses of liver sections from vehicle- and ConA-treated immunocompromised mice. Scale bars represent 50 microns. Transverse PET/CT images (B) and quantification (C) of vehicle- and ConA-treated immunocompromised mice injected with ^{18}F-FDG, ^{18}F-FAC, and ^{18}F-DFA. Livers are outlined in a white dotted line. Quantification represents radiotracer accumulation in the liver normalized to a background organ. ns: not significant.

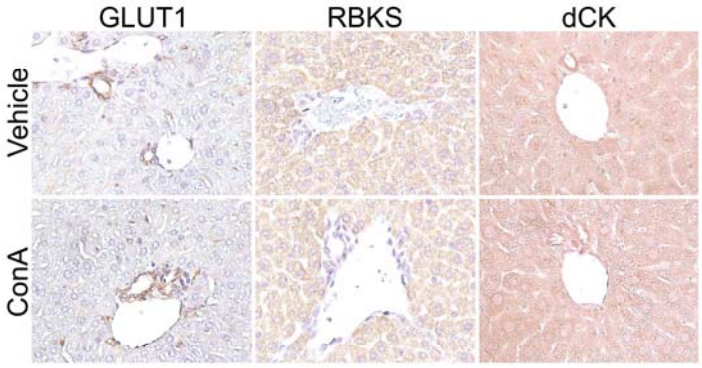

Figure S3: GLUT1, RBKS, and dCK protein levels are unaffected in liver sections from immunocompromised mice treated with ConA compared to vehicle-treated mice. GLUT1, RBKS, and dCK immunostained vehicle- and ConA-treated immunocompromised mouse liver sections.

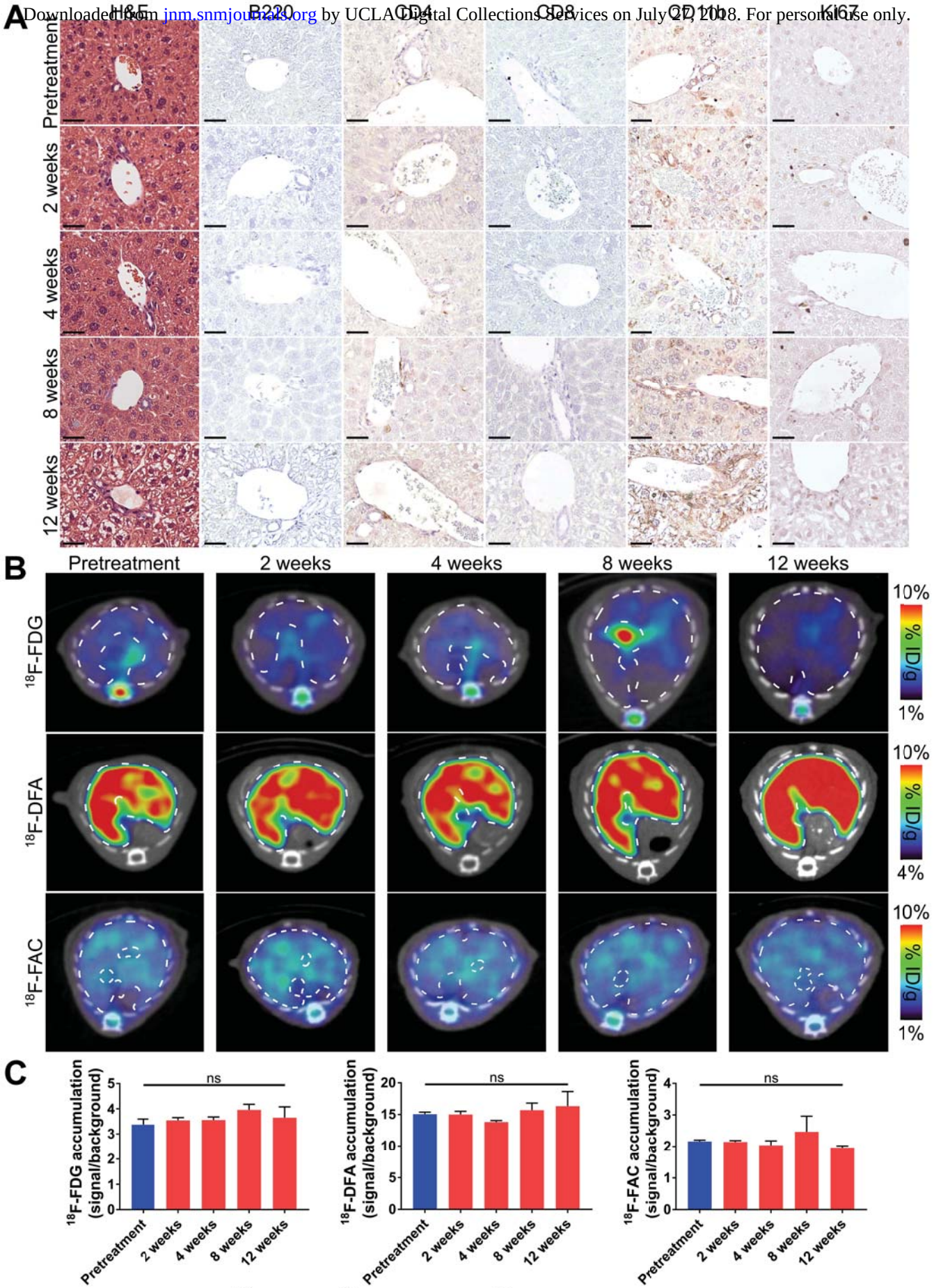

Figure S4: Hepatic ^{18}F-FDG, ^{18}F-FAC, and ^{18}F-DFA accumulation are unaffected in immunocompromised mice treated with adenovirus. (A) Histological and immunohistochemical analyses of liver sections from pretreatment and adenovirus-treated immunocompromised mice. Scale bars represent 50 microns. Transverse PET/CT images (B) and quantification (C) of pretreatment and adenovirus-treated immunocompromised mice injected with ^{18}F-FDG, ^{18}F-DFA, and ^{18}F-FAC. Quantification represents radiotracer accumulation in the liver normalized to a background organ. ns: not significant.

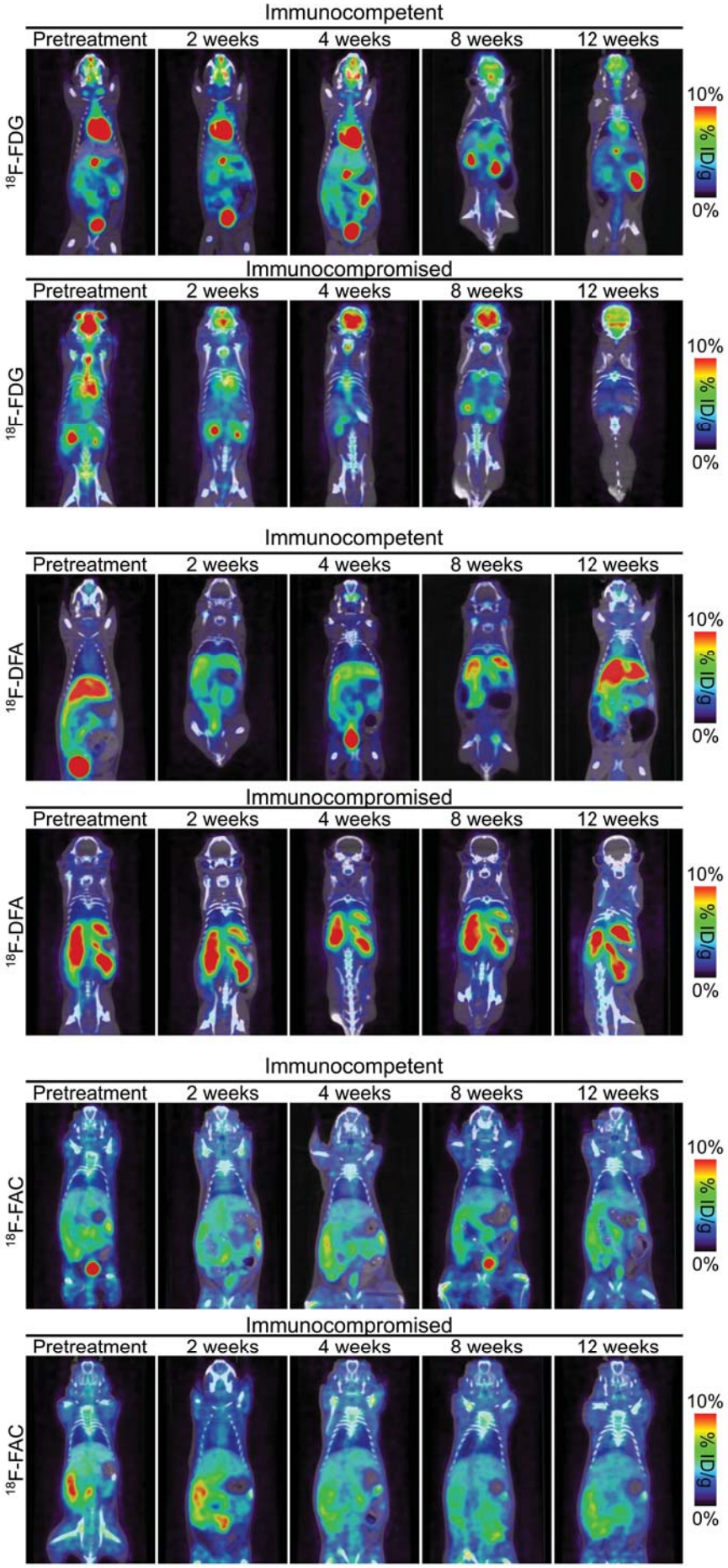

Figure S5: ^{18}F-FDG, ^{18}F-FAC, and ^{18}F-DFA accumulation in a mouse model of viral hepatitis. Representative coronal sections of pretreatment and adenovirus-treated mice injected with ^{18}F-FDG, ^{18}F-DFA, and ^{18}F-FAC.

JNM The Journal of NUCLEAR MEDICINE

^{18}F-FAC PET selectively images hepatic infiltrating CD4 and CD8 T cells in a mouse model of autoimmune hepatitis

Jessica R. Salas, Bao Ying Chen, Alicia Wong, Donghui Cheng, John S. Van Arnam, Owen N. Witte and Peter M. Clark

J Nucl Med.
Published online: April 26, 2018.
Doi: 10.2967/jnumed.118.210328

The Journal of Nuclear Medicine is published monthly.
SNMMI | Society of Nuclear Medicine and Molecular Imaging
1850 Samuel Morse Drive, Reston, VA 20190.
(Print ISSN: 0161-5505, Online ISSN: 2159-662X)

SNMMI SOCIETY OF NUCLEAR MEDICINE AND MOLECULAR IMAGING